The effect of wind speed products and wind speed–gas exchange relationships on interannual variability of the air–sea CO$_2$ gas transfer velocity

By ARE OLSEN[1,2]*, RIK WANNINKHOF[3], JOAQUIN A. TRIÑANES[4] and TRULS JOHANNESSEN[1,2], [1]*Geophysical Institute, University of Bergen, Allégaten 70, 5007 Bergen, Norway;* [2]*Also at Bjerknes Centre for Climate Research, Allégaten 55, 5007 Bergen, Norway;* [3]*NOAA Atlantic Oceanographic and Meteorological Laboratory, 4301 Rickenbacker Causeway, Miami, FL 33149, USA;* [4]*Technological Research Institute, University of Santiago de Compostela, Santiago de Compostela, 15782, Spain*

ABSTRACT

The lack of a firm relationship between wind speed (U_{10}) and gas transfer velocity (k) is considered to be one of the factors that hinders accurate quantification of interannual variations of ocean–atmosphere CO$_2$ fluxes. In this paper the interannual variations of k of using four different k–U_{10} parametrizations are examined using wind speed data from the NCEP/NCAR reanalysis project. The extent to which interannual variations are faithfully reproduced in the NCEP/NCAR data is also investigated. This is carried out through comparison with QuikSCAT data. Compared with 4 yr of QuikSCAT data, NCEP/NCAR data reproduce interannual k variations, although the absolute magnitude of k is underestimated. Interannual k variation shows great sensitivity to selection of k–U_{10} parametrization, and in the Westerlies it changes by a factor of three depending on k–U_{10} parametrization. Use of monthly mean winds speeds leads to overestimation of interannual k variations compared with k variations computed using 6-hourly wind speeds and the appropriate k–U_{10} parametrization. Even though the effect of changing k–U_{10} parametrization is large enough to be an issue that needs to be considered when computing interannual air–sea CO$_2$ flux variations through combining estimates of k with data for the air–sea CO$_2$ gradient, it is not sufficient to bridge the gap between such estimates and estimates based on analyses of atmospheric oxygen, CO$_2$ and δ^{13}C data. Finally it is shown that the ambiguity in the relationship between wind speed and k introduces an uncertainty in interannual flux variations comparable to a bias of interannual ΔpCO$_2$ variations of at most ± 5 μatm.

1. Introduction

The growth rate of the atmospheric CO$_2$ concentration is determined not only by the magnitude of the emissions from fossil fuel combustion but also by ocean and terrestrial CO$_2$ uptake. In fact, even though emission rates stayed almost constant throughout the 1990s, the growth rate of atmospheric CO$_2$ ranged from 0.6 to 2.6 ppm yr^{-1} (Marland and Boden, 2001). The annual CO$_2$ emissions averaged around 6 ± 1 gigatonne of carbon (Gt C) which translates into an atmospheric burden of about 2.7 ppm yr^{-1}. Thus the annual uptake efficiency—with respect to the anthropogenic carbon release—of the combined land and ocean carbon sink varied between 5 and 80% over the last decade. A better mechanistic understanding of this variability will enhance our ability to predict the future behaviour of car-

bon sinks, which is essential for forecasting climate change. As of now, not even the magnitude of the variability of each reservoir is very well known. Variability of the ocean CO$_2$ sink has been found to be substantial, with peak to peak variations being around ± 1 Gt C or more when using top-down approaches that utilize observations of atmospheric CO$_2$, O$_2$ and δ^{13}C (Battle et al., 2000; Bousquet et al., 2000; Le Quéré et al., 2003). On the other hand, when global ocean circulation–biogeochemistry models have been employed to compute interannual variability of the ocean CO$_2$ uptake (bottom-up), peak to peak variations of only around ± 0.5 Gt C are determined (Le Quéré et al., 2000, 2003; Obata and Kitamura, 2003). Similar small interannual variations of ocean CO$_2$ uptake were also estimated in a study that used sea surface temperature (SST) as a proxy for ΔpCO$_2$ (Lee et al., 1998). As bottom-up approaches rely on use of an air–sea gas transfer velocity term (k), parametrized as a function of the wind speed 10 m above the sea surface (U_{10}) (Liss and Merlivat, 1986; Wanninkhof, 1992; Wanninkhof and

*Corresponding author.
e-mail: are.olsen@gfi.uib.no

McGillis, 1999), underestimation of the variability of k is one potential reason why these approaches tend to yield lower inter-annual variations of ocean CO_2 uptake than top-down methods. Underestimation of k variations can be caused by a number of factors, including the use of smoothed reanalysed fields of wind speed, too low a sensitivity of the transfer velocity equation to wind speed variations and insufficient temporal resolution of the wind speed product used. These issues are the subject of the present paper.

The rest of this paper is divided into six sections. First (Section 2) the data and the methods used to compute air–sea CO_2 gas transfer velocities are described. Then (Section 3) we evaluate if use of reanalysed wind speed data underestimates magnitude and variability of gas transfer velocities. In Section 4 the effect of using different k–U_{10} parametrizations on inter-annual variability of k is examined. This includes an evaluation of the effect of using short-term (6-hourly) versus long-term (monthly) wind speeds. Section 5 addresses the consequences of changing k–U_{10} parametrization for estimates of interannual air–sea CO_2 flux variability and Section 6 evaluates the significance of this effect in terms of $\Delta p CO_2$. A summary of the findings is presented in Section 7.

2. Data and Methods

Wind speed data from the NCEP/NCAR reanalysis project (Kalnay et al., 1996) were obtained from the web site of the NOAA-CIRES Climate Diagnostics Center, Boulder, CO, USA (http://www.cdc.noaa.gov/). Wind speeds at 10 m above the sea surface (U_{10}) were computed from the 6-hourly wind vector product that is supplied on a T62 Gaussian grid, corresponding to approximately 1.9° in both latitude (lat) and longitude (lon). These data are henceforth referred to as NCEP wind speeds, and cover the time period from 1948 until the present.

Wind speed data from the SeaWinds sensor on board the QuikSCAT satellite were obtained from the Physical Oceanography Distributed Active Archive Center of the Jet Propulsion Laboratory (http://podaac.jpl.nasa.gov). This instrument measures radar backscatter and retrieves wind speed and direction at a height of 10 m over the ocean surface. For this work we used the level 2B swath product that has a resolution of 25 km. All rain-flagged observations were eliminated from the data set. Throughout this paper we will refer to these data as QuikSCAT winds.

Analysed fields of monthly mean bias corrected satellite SST were obtained from the IRI/LDEO Climate Data Library (http://ingrid.ldgo.columbia.edu/). These fields have been created following Reynolds and Smith (1994), and are henceforth referred to as the Reynolds and Smith SST. These data are available from November 1981.

Fields of monthly mean surface ocean $\Delta p CO_2$, the difference between atmospheric and surface ocean CO_2 partial pressure ($p CO_2^{atm} - p CO_2^{sw}$), normalized to the year 1995 were supplied

by Dr T. Takahashi of the Lamont-Doherty Earth Observatory, Columbia University (Takahashi et al., 2002). These data, henceforth referred to as the Takahashi $\Delta p CO_2$ data, were supplied on a 4°lat × 5°lon grid. All calculations have been carried out on this grid. The SST data were bin-averaged to fit the grid.

The monthly mean air–sea CO_2 gas transfer velocity, k, has been computed according to four different parametrizations:

$$k_{\text{LM\_86}} = \frac{\sum (a U_{10} + b)}{n} \left(\frac{Sc}{600} \right)^{-c} \tag{1}$$

$$k_{\text{W92\_i}} = 0.31 \frac{\sum U_{10}^2}{n} \left(\frac{Sc}{660} \right)^{-1/2} \tag{2}$$

$$k_{\text{W92\_av}} = 0.39 U_{10,\text{av}}^2 \left(\frac{Sc}{660} \right)^{-1/2} \tag{3}$$

$$k_{\text{WM99\_i}} = 0.0283 \frac{\sum U_{10}^3}{n} \left(\frac{Sc}{660} \right)^{-1/2}. \tag{4}$$

Equation (1) follows Liss and Merlivat (1986), and the coefficients a, b and c are dependent on the wind speed range. Equation (2) follows the Wanninkhof (1992) formulation for short-term winds, eq. (3) follows the Wanninkhof (1992) formulation for time-averaged winds and eq. (4) follows the Wanninkhof and McGillis (1999) formulation for short-term winds. The formulation of Wanninkhof and McGillis (1999) for time-averaged winds was not used since it appears to significantly overestimate the gas transfer velocity (Wanninkhof et al., 2002). For the NCEP winds, the 6-hourly wind speed data bin averaged to 4°lat × 5°lon were used for U_{10}, and n is the number of wind speed data each month. For the QuikSCAT winds, the individual wind speed retrievals were used for U_{10}, and n is the number of retrievals each month in each 4°lat × 5°lon grid cell. The Schmidt number, Sc, was computed from monthly SSTs according to Wanninkhof (1992).

Quarterly averaged latitudinal profiles of k, its interannual standard deviation and other derived values are presented throughout this paper. All of these profiles have been computed from the monthly pixel estimates of the parameter in question by averaging over each latitude band and then over each quarter.

Indication of season refers to the corresponding Northern Hemisphere season unless otherwise noted.

3. Estimates of the air–sea gas transfer velocity, QuikSCAT versus NCEP

The NCEP wind speed data are hindcast using observations from a number of sources and a frozen data assimilation system (Kalnay et al., 1996). Use of NCEP data for computation of magnitude and variability of k can be problematic. For instance, Smith et al. (2001) showed that the NCEP wind speed data are biased when compared with wind speed data collected during the World Ocean Circulation Experiment. At very low wind speeds NCEP winds have a positive bias of around 1 m s^{-1}, but when wind speeds are higher than 5 m s^{-1}, the bias

increases linearly from -0.5 m s^{-1} and reaches -5 m s^{-1} at wind speeds of 18 m s^{-1}. Smith et al. (2001) attributed this to too smooth pressure gradients in the NCEP/NCAR product. Given the smooth nature of the NCEP wind speeds it has been suggested that they also underestimate interannual variability (Carr et al., 2002). A validation of the magnitude and variability of transfer velocities computed from NCEP wind speed data is therefore appropriate. This is carried out through comparison with transfer velocities computed from QuikSCAT data. These data are often considered the current best remotely sensed wind speed product. Chelton et al. (2001) compared QuikSCAT data with data from the Tropical Atmosphere–Ocean (TAO) buoys in the eastern tropical Pacific and found that the QuikSCAT data were on average 0.74 m s^{-1} lower than the TAO data. The small bias of QuikSCAT data has been confirmed in a study of winds over the Indian Ocean (Goswami and Sengupta, 2003), a study that also revealed a significant negative bias in NCEP wind speeds.

Monthly mean values of k computed using NCEP data are compared with values of k computed from QuikSCAT data. This comparison is restricted to data from the years when QuikSCAT data are available, i.e. 2000, 2001, 2002 and 2003. All rain-flagged QuikSCAT observations were removed from the data set and a lower limit of 10 000 observations per month per 4°lat × 5°lon pixel was invoked in order to ensure that the monthly mean ks were based on data from more than 20 d each month. In order to avoid bias of the results, only grid cells that had a sufficient coverage of QuikSCAT data in all years were used in the comparison; this procedure removed approximately 10% of the pixels, mostly at high latitudes.

Before embarking on a description of the results it is worthwhile to briefly introduce the zonal structure and features of the major marine wind systems since these will be referred to throughout this article. The doldrums are the weak winds centred on the equator. The trade winds are the stronger surface winds centred on 15° in the Southern and Northern Hemisphere flowing towards the equator with an easterly component in its direction. The horse latitudes are zones of light winds centred at around 30° in each hemisphere. Finally, the Westerlies are broad zones of strong and persistent west to east winds at about 50° in the Southern and Northern Hemisphere.

Figure 1 shows quarterly averaged latitudinal profiles of the 2000–2003 NCEP and QuikSCAT based estimates of k_{W92_i} and their interannual standard deviation.

Figure 1 shows that use of NCEP wind speed underestimates k_{W92_i} relative to QuikSCAT data during all seasons and over all latitude bands. The difference is greatest in the doldrums and up to the trades in both hemispheres, around 4 to 7 cm h^{-1}, and asymmetric around the equator in that it is normally larger to the north than to the south. In the Northern Hemisphere the smallest differences are found around 50°N where there is no bias of k_{W92_i} in the third quarter and a bias of only -1 to -2 cm h^{-1} throughout the rest of the year. To the north of this, bias is normally larger, around -3 to -4 cm h^{-1}, and only slightly

lower in the summer half of the year than in the winter half. To the south of 50°N, through the horse latitudes to the trade wind region, the bias of k_{W92_i} is similar to the bias north of 50°N. In the Southern Hemisphere the smallest bias is also found around 50°, around -1 cm h^{-1} or less during the austral summer half of the year and increasing to around -2 cm h^{-1} in winter. The bias in the southern horse latitudes and trades is of similar magnitude as the bias in the north. Finally, the bias is quite large in the southernmost latitudes, up to -5 cm h^{-1}.

The differences in transfer velocities that are seen here are mainly a result of differences in wind speeds of around 1.5 m s^{-1} around the equator, 0.5–1 m s^{-1} up to 60° (north and south) and 1–3 m s^{-1} at latitudes higher than 60° (not shown). The high spatial resolution of the QuikSCAT winds compared with the NCEP winds may also contribute to the difference; this has not been evaluated.

As regards interannual variations, no significant differences between NCEP and QuikSCAT are evident (Fig. 1). Thus even though NCEP winds are lower than QuikSCAT, their interannual variability appears similar. It has been suggested that the use of reanalysed fields of wind speed underestimates interannual variability of the air–sea CO$_2$ exchange coefficient (Carr et al., 2002). Our results show that when compared with scatterometer winds this is not the case, and NCEP winds gives adequate estimates of interannual k variations.

The effect on the air–sea CO$_2$ flux of the difference between QuikSCAT- and NCEP-derived transfer velocities was quantified by applying the fields of k_{W92_i} on the $\Delta p\mathrm{CO}_2$ field of Takahashi et al. (2002) and computing the air–sea CO$_2$ flux, F, through:

$$F = Sk\Delta p\mathrm{CO}_2. \tag{5}$$

The estimates of solubility, S, were also obtained from Takahashi et al. (2002). The NCEP data gave an average annual ocean carbon uptake of 1.68 Gt C with an interannual standard deviation of 0.003 Gt C, and the QuikSCAT data gave a slightly lower uptake, 1.59 Gt C but with the same interannual standard deviation, 0.003 Gt C. The lower uptake computed with the QuikSCAT data is a result of higher transfer velocities at low latitudes. Note that these estimates are slightly biased towards low latitudes since about 10% of the pixels have been removed as described above. (See section 5 for estimates of the global net flux.)

4. Effect of using different k–U_{10} parametrizations on interannual variability of k

Monthly mean gas transfer velocities were computed using NCEP data and either eq. (1), eq. (2), eq. (3) or eq. (4). The calculations span the time period November 1981 to December 2002. Figure 2 shows quarterly averaged latitudinal profiles of monthly mean transfer velocities. The sensitivity of k to different k–U_{10} parametrizations is well known (Wanninkhof and McGillis, 1999; Boutin et al., 2002). k_{W92_i} is larger than k_{LM86_i}
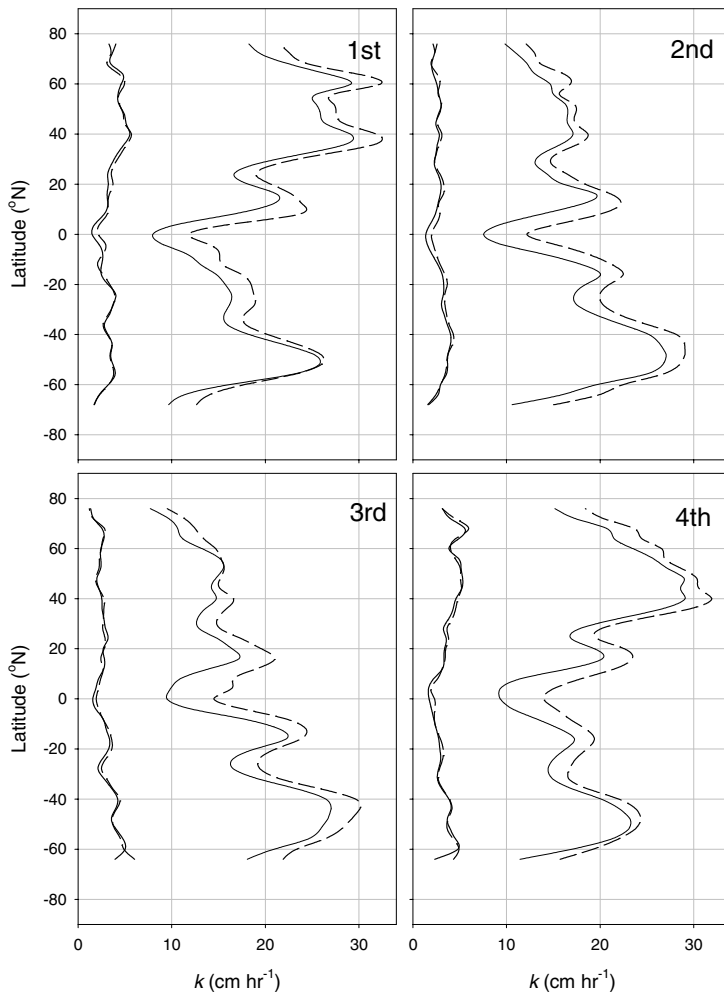
Fig 1. Quarterly averaged profiles of k_{W92_i} (two curves to the right in each panel) and its interannual standard deviation 2000–2003 (two curves to the left) computed using NCEP and QuikSCAT wind speed data (NCEP, full curve; QuikSCAT, dashed curve).

at all wind speeds, and the difference between these two increases with increasing wind speed because of the quadratic nature of the wind speed dependency of k_{W92_i}. The cubic wind speed dependency of k_{WM99_i} makes it even more sensitive to changes in wind speed than k_{W92_i}, and it is lower than k_{W92_i} at wind speeds less than 11 m s^{-1}, lower than k_{LM86_i} at wind speeds between 3.5 and 7.5 m s^{-1} and similar to k_{LM86_i} below 3.5 m s^{-1}. The averaged transfer velocities computed using more than 20 yr of NCEP data confirm these features (Fig. 2). k_{WM99_i} is lower than k_{LM86_i} in the doldrums, but elsewhere k_{LM86_i} is lower than both k_{WM99_i} and k_{W92_i}. k_{W92_i} is normally larger than k_{WM99_i} but not in high-wind-speed regimes, such as the Westerlies during winter in both hemispheres. Moreover, the spans of the ks are different, illustrating the different sensitivity to change in wind speed. Whereas the k_{LM86_i} values span a range of 5–15 cm h^{-1} centred around 10 cm h^{-1}, k_{WM99_i} ranges from around 5 to over 30 cm h^{-1}. Compared with these two, k_{W92_i} has an intermediate span, from around 8 to 28 cm h^{-1}. The different sensitivity to change in wind speed is also illustrated in the seasonal variations of the transfer velocities; the k_{LM86_i} values exhibit the

lowest seasonal variations and the k_{WM99_i} values exhibit the largest seasonal variations.

The transfer velocities all exhibit the same pattern of interannual variability, both geographical and seasonal but to various degrees (Fig. 3). It is large in the northern Westerlies with a clear seasonal variation, largest in the winter and lowest in the summer half of the year. The interannual standard deviation decreases moving south into the horse latitudes and increases again in the trade wind region, but it does not reach the same magnitude as in the Westerlies. The smallest interannual variation occurs in the doldrums. The interannual standard deviation in the Southern Hemisphere varies less with season than in the Northern Hemisphere, but the geographical features are similar. Most variability is in the Westerlies; the horse latitudes show less variability, while the variability increases in the trades. A brief description of how k variations relate to the three major modes of climate variability, the Southern Oscillation, the Antarctic Oscillation and the Arctic Oscillation, is provided in the appendix. The pattern of distribution of the interannual variability is most pronounced for k_{W99_i}. It is less pronounced for k_{W92_i}, and weak and sometimes
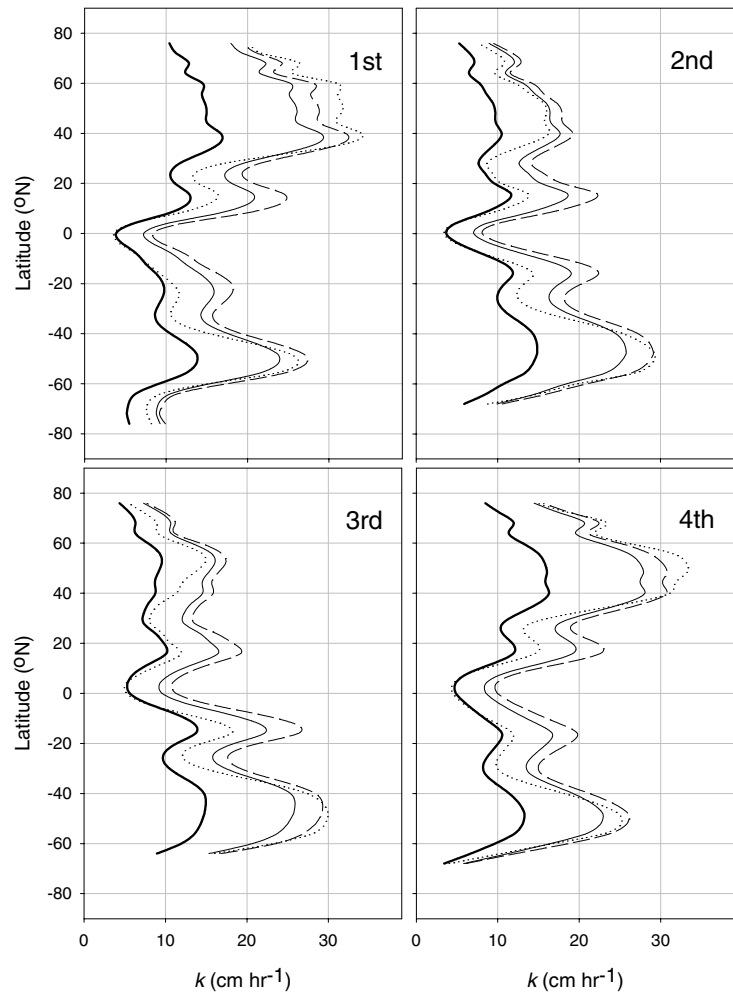
Fig 2. Quarterly averaged profiles of mean 1981–2002 CO$_2$ gas transfer velocities estimated from NCEP wind speed data using different k–U_{10} parametrizations: k_{LM86_i}, thick full curve; k_{W92_i}, thin full curve; k_{W92_av}, dashed curve; k_{WM99_i}, dotted curve.

even absent for k_{LM86_i}. This is a result of the different sensitivity to wind speed variations of the k–U_{10} parametrizations. The interannual standard deviation of k_{LM86_i} is only 1–3 cm h^{-1}, and corresponds to around 50 and 70% of the interannual standard deviation of k_{W92_i} (Fig. 4) in the Westerlies and doldrums, respectively. The interannual standard deviation of k_{WM99_i} ranges from 1 cm h^{-1} in the doldrums up to 10 cm h^{-1} in the northern Westerlies. Thus, it is 70% of that of k_{W92_i} in the former region and 50–70% greater in the latter. The interannual standard deviation of k_{W92_i} (Fig. 3) is around 2 cm h^{-1} in the doldrums, irrespective of season. In the northern Westerlies it is around 5 cm h^{-1} in winter, decreasing to 3 cm hr^{-1} in summer. The variability in the northern trades during summer is similar to that in the Westerlies, but during winter it is lower at around 4 cm h^{-1}. In the Southern Hemisphere variability of k_{W92_i} is around 2 cm h^{-1} in the trades and around 4 cm h^{-1} in the Westerlies.

The differences in the magnitude and interannual variability of k_{LM86_i}, k_{W92_i} and k_{WM99_i} are a consequence of the different assumptions used when fitting the k–U_{10} relationships to

the data: (1) the relationship of Liss and Merlivat (1986) consists of three linear segments of increasing slope, (2) that of Wanninkhof (1992) is quadratic and (3) that of Wanninkhof and McGillis (1999) is cubic. The difference between k_{W92_i} and k_{W92_av} is of a different nature; it arises because at a regional level the wind speed distribution departs from the Rayleigh distribution function that was employed when the relationship for long-term winds (k_{W92_av}) was deconvolved to a relationship for short-term winds (k_{W92_i}) (Wanninkhof, 1992). The global ocean wind speed distribution can be represented by a Rayleigh distribution function (Wentz et al., 1984), and this implies that the transfer velocities should be scaled with a factor of 1.25 when long-term rather than short-term winds are employed. However, Wanninkhof et al. (2002) showed that although this is true on a global basis, there is non-Rayleigh behaviour in many regions so that the correct scaling factor is frequently only 1.1–1.2. This overestimation of the scaling factor leads to an overestimation of both the magnitude of the transfer velocity (Fig. 2) and its interannual standard deviation (Fig. 3). Thus, k_{W92_av} is greater than k_{W92_i} at all latitudes and the difference is greatest in regions
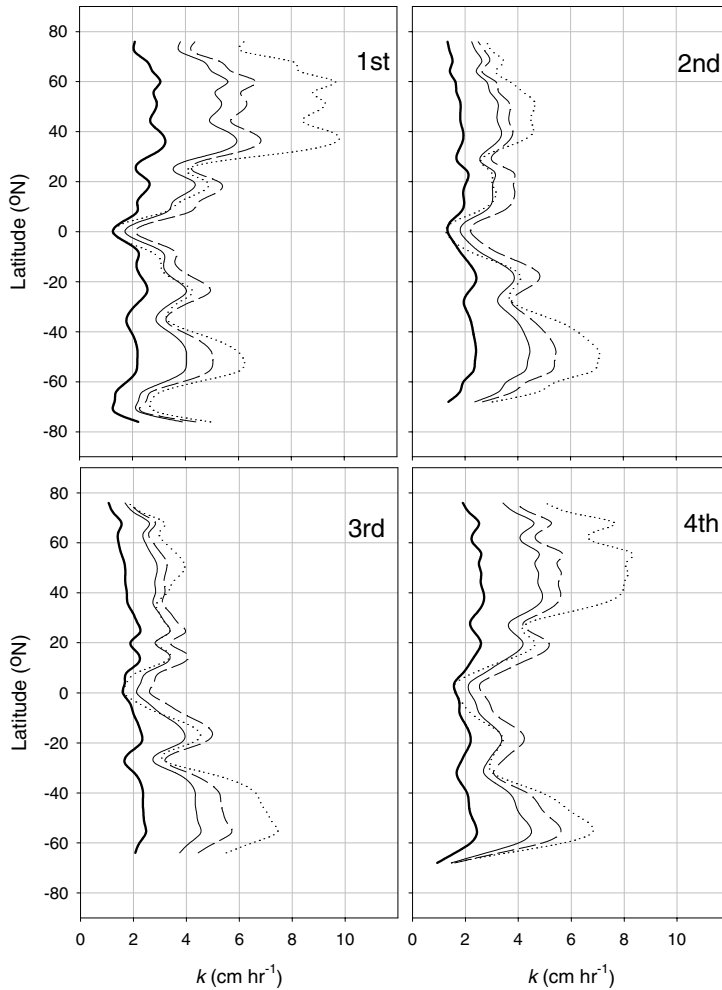
Fig 3. Quarterly averaged profiles of the 1981–2002 interannual standard deviation of CO_2 gas transfer velocities estimated from NCEP wind speed data using different k–U_{10} parametrizations: k_{LM86_i}, thick full curve; k_{W92_i}, thin full curve; k_{W92_av}, dashed curve; k_{WM99_i}, dotted curve.

that are dominated by steady winds, the trades and the southern Westerlies. The effect is so large in the southern Westerlies that k_{W92_av} is similar to or even exceeds k_{WM99_i} in austral summer (Fig. 2). The fractional increase in k following use of eq. (3) rather than eq. (2) (not shown) was similar to the increase estimated by Wanninkhof et al. (2002) who used wind speed data from a single year only (1995). Interannual variability using k_{W92_av} is overestimated by around 10–20% (Fig. 4). Thus, estimates of interannual variability of air–sea CO_2 exchange based on monthly mean wind speed data such as Olsen et al. (2003) and Bates (2002) appear to be overestimates.

Although the long-term k–U_{10} parametrization of Wanninkhof and McGillis (1999) has not been included in this study it is possible to infer the outcome if the calculations had been carried out using this. For this relationship the error and overestimation of k introduced with the Rayleigh assumption is greater than for k_{WM92_av}. Clearly use of the long-term Wanninkhof and McGillis (1999) relationship would overestimate interannual variability of transfer velocities relative to k_{WM99_i}.

5. Implications for estimates of variability of ocean CO_2 uptake

The results presented in Section 3 suggest that although the NCEP reanalysis data underestimate the absolute magnitude of k, they do not underestimate interannual variations of k. The effect of changing k–U_{10} parametrization is far more important, and in some regions interannual k variations may change by a factor of 3 or more when changing k–U_{10} parametrization (Section 4). The implications of this effect for estimates of variability of CO_2 exchange are discussed in this section.

The importance of k variations for variations of the global net flux is determined by applying the fields of k on the ΔpCO_2 field of Takahashi et al. (2002) and computing the air–sea CO_2 flux through eq. (5). This approach neglects any effects from potential correlation between interannual k and ΔpCO_2 variations.

The geographical pattern of the air–sea CO_2 flux and its sensitivity to selection of k–U_{10} parametrization (Fig. 5) follows the description of Boutin et al. (2002) and Wanninkhof et al. (2002).
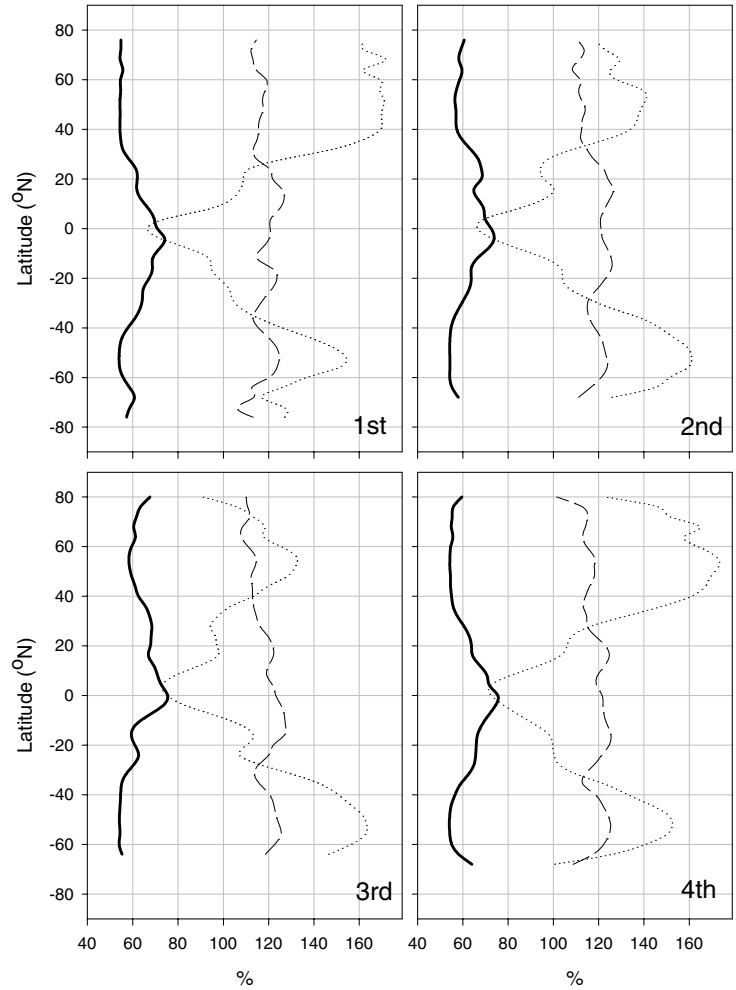
Fig 4. Quarterly averaged profiles of the percentage change of the interannual standard deviation of k following use of k–U_{10} parametrizations other than $k_{\text{W92\_i}}$: $k_{\text{LM86\_i}}$, thick full curve; $k_{\text{W92\_av}}$, dashed curve; $k_{\text{WM99\_i}}$, dotted curve.
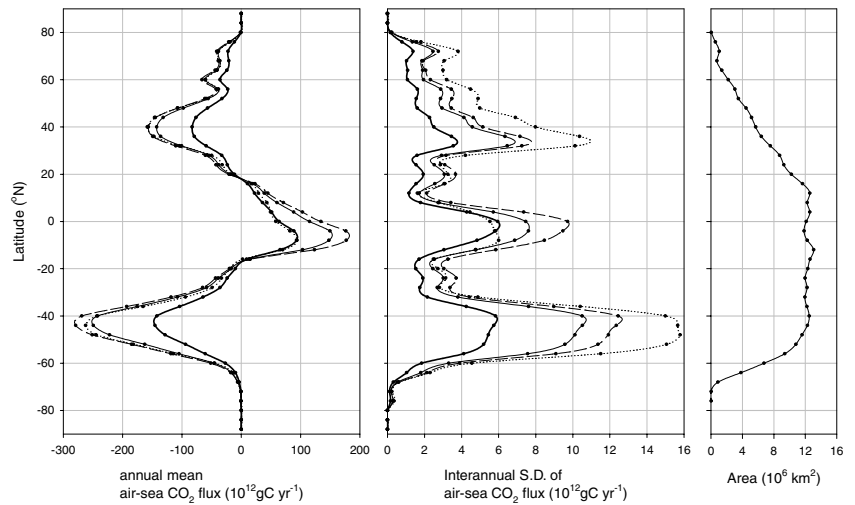

Fig 5. Latitudinal profiles of annual mean air–sea CO$_2$ exchange and the interannual standard deviation induced by k variations computed using NCEP winds, Takahashi ΔpCO$_2$ data and different k–U_{10} parametrizations: $k_{\text{LM86\_i}}$, thick full curve; $k_{\text{W92\_i}}$, thin full curve; $k_{\text{W92\_av}}$, dashed curve; $k_{\text{WM99\_i}}$, dotted curve. The panel to the right shows the zonal distribution of ocean surface area.

As an additional feature note that the fluxes computed using $k_{\text{W92\_av}}$ are greater than those computed using $k_{\text{WM99\_i}}$ around 40–50°S, because of the large deviation of the wind speed distribution from the Rayleigh distribution in this area. The largest ocean carbon uptake is estimated when $k_{\text{WM99\_i}}$ is used (Table 1), and this is more a consequence of the reduced outgassing in the lower latitudes rather than increased uptake at higher latitudes when compared with $k_{\text{W92\_i}}$ and $k_{\text{W92\_av}}$.

	F, k_{LM86_i}	F, k_{W92_i}	F, k_{W92_av}	F, k_{WM99_i}
Net flux	−1.00	−1.73	−1.86	−2.09
Interannual *SD*	0.04	0.06	0.07	0.09
Maximum flux	−1.07	−1.83	−1.99	−2.26
Minimum flux	−0.940	−1.61	−1.73	−1.92

Whereas the latitudinal profiles of interannual k variations had two distinct peaks associated with the Westerlies in each hemisphere (Fig. 3), the profiles of interannual variability of flux induced by k variations have an additional peak in the equatorial region (Fig. 5) and this a consequence of the inclusion of the ocean area and air–sea CO_2 gradient in the calculations. The equatorial region is characterized by a large air–sea CO_2 gradient and great area, and because of this, even small changes in k have strong impact on the total flux. Otherwise the geographical pattern of the interannual variability of flux induced by k variations is similar to that of the k variability. However, the interannual variability of flux induced by k variations around 60°N is less than expected from the variations of k; this follows from the small area of that region. The largest wind-induced variations of the flux takes place between 44 and 52°S, the southern mid-latitudes, a consequence of the variable Westerlies, the large ocean area and strong air–sea CO_2 gradient.

The interannual standard deviation of the flux induced by k variations is very sensitive to k–U_{10} parametrization (Fig. 5). At latitudes higher than 30° the use of k_{WM99_i} gives the largest wind-induced flux variations; up to around three times larger than when k_{LM86_i} is used. Of the three ks based on instant winds, k_{W92_i} gives the largest wind-induced flux variations in the equatorial region and k_{LM86_i} gives the lowest. Estimates of wind-induced interannual flux variations are most sensitive to selection of k–U_{10} parametrization in the mid-latitudes and the tropics. Use of k_{W92_av} gives larger wind-induced flux variations than k_{W92_i} at all latitudes, and this effect is greatest in the southern mid-latitudes and around the equator.

The effect of using different k–U_{10} parametrizations is apparent in the estimates of wind-induced interannual standard deviation of the global net flux over the 21 yr and ranges from 0.04 Gt C when k_{LM86_i} is used to 0.09 Gt C when k_{WM99_i} is used (Table 1). The peak to peak difference is 0.13 Gt C when k_{LM86_i} is used and 0.34 Gt C when k_{WM99_i} is used. These numbers can be contrasted with the model-based estimates of Le Quéré et al. (2000) and Obata and Kitamura (2003) of an interannual standard deviation of around 0.2 Gt C, and the empirical estimate of Lee et al. (1998). The effect of changing k–U_{10} parametrization is small compared with the variability of ocean CO_2 uptake inferred from atmospheric data where the peak to peak differences have been estimated to be around 2 Gt C (Battle et al., 2000; Bousquet et al., 2000). Thus, although selection of k–U_{10} parametrization is of

significance for estimates of interannual variations of ocean CO_2 uptake based on ocean data, underestimation of the variability of k does not seem to be the sole reason for the large difference between top-down and bottom-up estimates of flux variability.

6. Significance of changing k–U_{10} parametrization evaluated in terms of ΔpCO_2

It is worthwhile to put the results of Section 4 into a perspective with respect to ΔpCO_2, as this will allow for a better appreciation of the importance of the effect of changing k–U_{10} parametrization relative to what is known about ΔpCO_2 variability. In this section the change in interannual variability of ΔpCO_2 that has the same effect on flux variability as changing the k–U_{10} parametrization is determined.

Assume that only ΔpCO_2 varies, the standard deviation of the flux will then be given by:

$$\text{std}(F) = |S \times k|\text{std}(\Delta pCO_2.) \tag{6}$$

If, on the other hand, only k varies then:

$$\text{std}(F) = |S \times \Delta pCO_2|\text{std}(k). \tag{7}$$

In order to determine $\text{std}(\Delta pCO_2)$ that would give the same $\text{std}(F)$ as $\text{std}(k)$ we equate and rearrange eqs. (6) and (7) to:

$$\text{std}(\Delta pCO_2) = |\Delta pCO_2|\frac{\text{std}(k)}{k}. \tag{8}$$

The term $\text{std}(\Delta pCO_2)$ determined from eq. (8) is henceforth referred to as equivalent ΔpCO_2 variability and gives the interannual standard deviation of ΔpCO_2 that will cause as much standard deviation in fluxes as the variability of wind speeds.

Figure 6 presents quarterly averaged profiles of the equivalent ΔpCO_2 variability for k_{W92_i}, $\text{std}(\Delta pCO_2)_{W92\_i}$. In addition there are three more profiles in each panel of Fig. 6. These profiles show the change in ΔpCO_2 variability that has the same effect on interannual flux variations as changing the k–U_{10} parametrization from k_{W92_i} to one of the three other k–U_{10} parametrizations; k_{LM86_i}, k_{W92_av} or k_{WM99_i}. This latter term was computed following:

$$\Delta\text{std}(\Delta pCO_2)_x = \left|\overline{\Delta pCO_2}\right| \frac{\text{std}(k_{W92\_i})}{k_{W92\_i}} - \left|\overline{\Delta pCO_2}\right| \frac{\text{std}(k_x)}{k_{W92\_i}} \tag{9}$$

which can be derived in a similar manner as eq. (8). The x denotes the k–U_{10} parametrization that it is changed to. It is important to realize that whereas $\text{std}(\Delta pCO_2)$ is a measure of the importance of k variations in terms of ΔpCO_2, $\Delta\text{std}(\Delta pCO_2)_x$ is a measure of the uncertainty in interannual ΔpCO_2 variations that will introduce the same uncertainty in estimates of interannual flux variations as the uncertainty introduced by the existence of several k–U_{10} relationships.
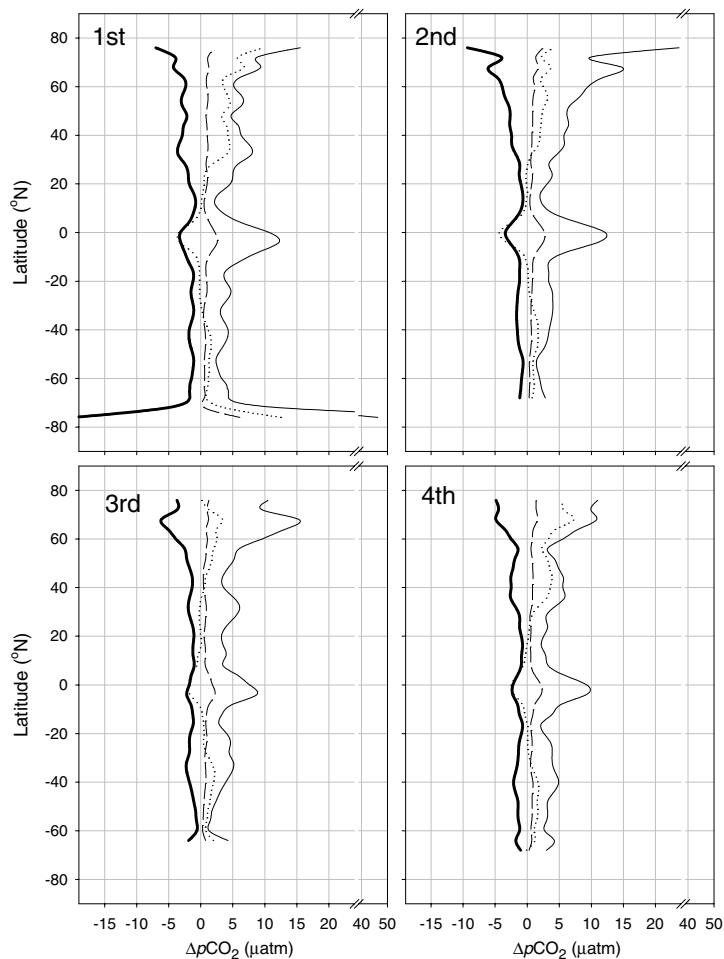
Fig 6. Equivalent ΔpCO_2 variability. The thin full curve in each panel is the quarterly averaged latitudinal profile of equivalent ΔpCO_2 variability for k_{W92_i} (std$(\Delta pCO_2)_{W92\_i}$). The three other profiles in each panel show the change of ΔpCO_2 variability that has a similar effect on interannual flux variations as changing from k_{W92_i} to one of the three other k–U_{10} parametrizations: Δstd$(\Delta pCO_2)_x$, $x =$ LM86_i, thick full curve; $x =$ W92_av, dashed curve; $x =$ WM99_i, dotted curve.

The std$(\Delta pCO_2)_{W92\_i}$ profiles in Fig. 6 illustrate what wind-speed-induced flux variations correspond to in variations of ΔpCO_2. The equivalent ΔpCO_2 variations for the three other k–U_{10} relationships (not shown) were very similar except that std$(\Delta pCO_2)_{WM94\_i}$ was around 4 μatm larger in the equatorial region and 3 μatm larger elsewhere, and that std$(\Delta pCO_2)_{LM86\_i}$ was around 3 μatm larger in the equatorial region. In the Northern Hemisphere variations in wind speed correspond in general to variations of ΔpCO_2 of around 5–10 μatm, but may increase up towards 15 μatm north of 60°N. The very high values seen close to 80°S in the first quarter and 80°N in the second is due to a few grid cells with a large air–sea CO_2 gradient and is neglected. Olsen et al. (2003) determined the interannual variability of Atlantic Ocean monthly mean wintertime ΔpCO_2 values north of 45°N to be at most 10 μatm and Gruber et al. (2002) determined interannual variations of ΔpCO_2 in the Sargasso Sea to be only a few ppm. These values are similar to the std$(\Delta pCO_2)_{W92\_i}$ values for the latitude bands in question. The equivalent ΔpCO_2 standard deviation peaks in the equatorial region at about 10 μatm, but it is still much less than the large variability of 50–100 μatm driven by the El Niño–Southern Oscillation system (Feely et al.,

2002; Cosca et al., 2003). In the Southern Hemisphere equivalent ΔpCO_2 variations are low, less than 5 μatm, and south of 40°S they are only around 3–4 μatm. At the same time this is the region where wind variation causes the largest interannual flux variations (Fig. 5). These results show that the ocean CO_2 uptake in the southern mid-latitudes is very sensitive to interannual ΔpCO_2 variations, a result of large area and the high k values.

The profiles of Δstd$(\Delta pCO_2)_x$ shown in Fig. 6 were computed relative to k_{W92_i}. Thus, Δstd$(\Delta pCO_2)_{LM86\_i}$ shows the decrease of ΔpCO_2 variability that will decrease interannual flux variations as much as changing k–U_{10} parametrization from k_{W92_i} to k_{LM86_i}; Δstd$(\Delta pCO_2)_{W92\_av}$ shows the increase of ΔpCO_2 variability that is required to increase interannual flux variations as much as changing k–U_{10} parametrization from k_{W92_i} to k_{W92_av}; and Δstd$(\Delta pCO_2)_{WM99\_i}$ shows the increase/decrease of ΔpCO_2 variability that will introduce similar changes in interannual flux variations as changing from k_{W92_i} to k_{WM99_av}. Fig. 6 shows that the Δstd$(\Delta pCO_2)_x$ values are all low, exceeding 5 μatm only in a few northern high-latitude grid cells. This means that changing the k–U_{10} parametrization from k_{W92_i} to any of the three others has the same effect on interannual flux variations as a change in

the interannual variability of $\Delta p CO_2$ at a large scale of less than 5 μatm. In other words, the uncertainty introduced in estimates of the interannual variations of the air–sea CO_2 flux because of the lack of a firm relationship between wind speed and gas transfer velocity corresponds to an uncertainty in interannual variations of $\Delta p CO_2$ of at most ± 5 μatm. This is less than the precision of current estimates of regional $p CO_2$ distributions and their inter-annual variability (Etcheto et al., 1999; Louanchi and Hoppema, 2000; Nelson et al., 2001; Olsen et al., 2003; Cosca et al., 2003; Olsen et al., 2004). Thus, it is clear that at present inaccuracies in the estimates of $\Delta p CO_2$ rather than transfer velocity constitute the biggest limitation on our ability to estimate the interannual variations of ocean CO_2 uptake.

7. Summary

The most important results on interannual variations of k that have been presented in this study can be summarized in the following points:

(1) Use of NCEP/NCAR wind speed data underestimates the absolute magnitude of the gas transfer velocity compared with QuikSCAT data by between 1 and 7 cm h^{-1}, depending on latitude, but the interannual standard deviation is not underestimated (Fig. 1).

(2) Estimates of interannual variations of k are sensitive to selection of the wind speed–gas transfer relationship, and in some regions a change of k–U_{10} parametrization will cause the interannual k variability to change by a factor of 3. Of the three relationships based on short-term winds k_{LM86_i} gives the lowest interannual variations and k_{W92_i} yields the greatest variations at latitudes lower than 15–25° (N and S); elsewhere k_{WM99_i} yields the greatest variability (Fig. 3). Use of monthly averaged wind speeds (i.e. use of k_{W92_av} instead of k_{W92_i}) leads to the over-estimation of interannual k variations by between 10 and 20% depending on latitude (Fig. 4).

(3) The magnitude of the interannual k variations is most sensitive to selection of k–U_{10} parametrization in the Westerlies (Figs. 3 and 4), but wind-induced flux variations are also very sensitive to selection of k–U_{10} parametrization in the tropics (Fig. 5).

(4) Wind-speed-induced variation of the global net flux may vary by a factor of more than 2, from 0.04 to 0.09 Gt C, depending on the k–U_{10} parametrization used (Table 1). This makes selection of the k–U_{10} parametrization an issue worthy of consideration for bottom-up estimates of interannual flux variations; however, the effect is far too small to be the only factor that can reconcile bottom-up with top-down estimates of flux variations.

(5) Wind-speed-induced flux variations correspond to an interannual variability of $\Delta p CO_2$ of 2–10 μatm, and the lack of a firm relationship between wind speed and gas transfer velocity corresponds to an uncertainty of interannual $\Delta p CO_2$ variations of less than 5 μatm over all latitude bands (Fig. 6).

9. Appendix: Gas transfer velocity variability and the three major modes of climate variations

Maps illustrating the relationship between interannual k variations and major modes of climate variability are presented in this appendix. These maps are not directly related to the main issue of this paper but will still be of general interest to the CO_2 research community and are therefore presented here as supplementary material. The maps are presented in Figs 7a–c , and show the correlation coefficient (r) between monthly values of k_{W92_i} (based on NCEP winds) and (a) the Southern Oscillation Index (SOI), (b) the Antarctic Oscillation Index (AAOI) and (c) the Arctic Oscillation Index (AOI). The seasonal signal in both k and the climate indices was removed by, for each month, removing the long-term monthly mean from the monthly values.

The SOI is defined as the normalized pressure difference between Tahiti and Darwin, and it is closely associated with the strength of the trade winds over the Pacific Ocean. When the SOI is positive (La Niña conditions) there are strong trades blowing east to west over the Pacific; when the SOI goes to negative values (El Niño conditions) the trades are weakened and sometimes even reversed. There are also more far-reaching effects of the Southern Oscillation—Northern Hemisphere trades in the Atlantic Ocean are weakened during negative SOI states as is also the mid-latitude Westerlies in the Southern Hemisphere (Van Loon and Madden, 1981). All of these features are recognized in Fig. 7a with positive correlations between the SOI and gas transfer velocities in the Tropical Pacific, Tropical Atlantic and in the Westerlies zone of the South Eastern Pacific. The impact of the Southern Oscillation on interannual k variability is largest in the Southern Pacific.

The Arctic and Antarctic Oscillations or Northern and Southern Hemisphere annular modes are the leading modes of high-latitude climate variability in the respective hemisphere. Both of these modes manifest themselves as a see-saw in mean sea level pressure between high and middle latitudes (Thompson and Wallace, 2000). The annular modes are clearly of importance for
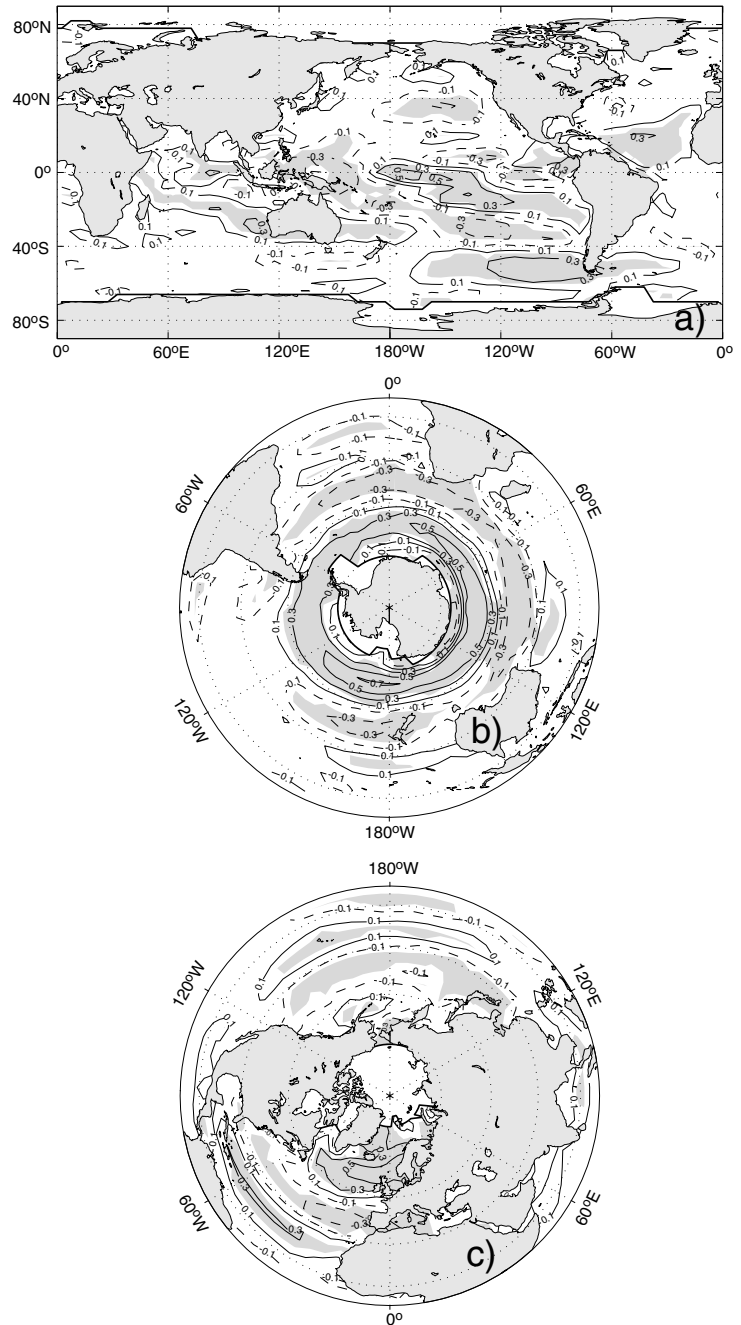
Fig 7. Correlation coefficient for the linear regression between anomalies of k_{W92_i} and anomalies of (a) the Southern Oscillation Index (SOI), (b) the Antarctic Oscillation Index (AAOI) and (c) the Arctic Oscillation Index (AOI). The grey shaded areas show regions where the slope of the regression is different from zero at a 99% confidence level. The SOI data were obtained from the Climate Research Unit of the University of East Anglia and have been computed following the method of Ropelewski and Jones (1987). The AAOI/AOI data were obtained from the National Weather Service of the National Ocean and Atmospheric Administration (NOAA/NWS) and were constructed by projecting the daily (00Z) 1000 mbar height anomalies poleward of 20°S/N onto the loading pattern of the AAOI/AOI.

interannual k variations (Figs 7b and c). In the Southern Hemisphere the regression reveals the zonal symmetric response of k to AAOI variations as a see-saw between high and middle latitudes. The response of Northern Hemisphere k to variations in the AOI is not as zonally symmetric, being strongest over the North Atlantic Ocean. Here there is a clear three-banded AOI signature in interannual k variability, with a positive relationship between AOI and k north of 60°N, a negative relationship between 30 and 45°N and a positive relationship between 10 and 30°N.

Even though statistical relationships between the three major modes of climate variability and interannual k variations have been identified, it is noteworthy that the regression coefficients are quite low, at most 0.5–0.7, and around 0.3–0.5 over large ocean areas. This means that a linear regression between the climate indices and interannual k variations explains only 10–50% of the latter. This result is in accordance with, for instance, the regression diagnostics obtained by Cayan (1992) for the linear regression between the North Atlantic Oscillation, the Atlantic manifestation of the AO, and wind speeds. Climate modes

should not therefore be regarded as the sole cause of interannual k variations, but rather as drivers of the large-scale underlying trends.

References

Bates, N. R., 2002. Interannual variability in the global uptake of CO_2. *Geophys. Res. Lett.* **29**, doi:1029/2001GL0013571.

Battle, M., Bender, M. L., Tans, P. P., White, J. W. S., Ellis, J. T. et al. 2000. Global carbon sinks and their variability inferred from atmospheric O_2 and δ^{13}C. *Science* **287**, 2467–2470.

Bousquet, P., Peylin, P., Ciais, P., Le Quere, C., Friedlingstein, P. et al. 2000. Regional changes in carbon dioxide fluxes of land and oceans since 1980. *Science* **290**, 1342–1346.

Boutin, J., Etcheto, J., Merlivat, L. and Rangama, Y. 2002. Influence of gas exchange coefficient parameterization on seasonal and regional variability of CO_2 air–ea fluxes. *Geophys. Res. Lett.* **29**. doi:10.1029/2001GL013872.

Carr, M.-E., Tang, W. and Liu, W. T. 2002. CO_2 exchange coefficients from remotely sensed wind speed measurements: SSM/I versus QuikSCAT in 2000. *Geophys. Res. Lett.* **29**, doi:10.1029/2002GL015068.

Cayan, D. C. 1992. Latent and sensible heat flux anomalies over the Northern Oceans: the connection to monthly atmospheric circulation. *J. Clim.* **5**, 354–369.

Chelton, D., Esbensen, S. K., Schlax, M. G., Thum, N., Freilich, M. H. et al. 2001. Observations of coupling between surface wind stress and sea surface temperature in the eastern Tropical Pacific. *J. Clim.* **14**, 1479–1498.

Cosca, C. E., Feely, R. A., Boutin, J., Etcheto, J., McPhaden, M. J. et al. 2003. Seasonal and interannual CO_2 fluxes for the central and eastern equatorial Pacific Ocean as determined from fCO_2–SST relationships. *J. Geophys. Res.* **108**, doi:10.1029/2000JC000677.

Etcheto, J., Boutin, J., Dandonneau, Y., Bakker, D. C. E., Feely, R. A. et al. 1999. Air–sea CO_2 flux variability in the equatorial Pacific Ocean near 100°W. *Tellus* **51B**, 734–747.

Feely, R. A., Boutin, J., Cosca, C. E., Dandonneau, Y., Etcheto, J. et al. 2002. Seasonal and interannual variability of CO_2 in the equatorial Pacific. *Deep Sea Res. II*, **49**, 2443–2469.

Goswami, B. N. and Sengupta, D. 2003. A note on the deficiency of NCEP/NCAR reanalysis surface winds over the Indian Ocean. *J. Geophys. Res.* **108**, doi:10.1029/2002JC001497.

Gruber, N., Keeling, C. D. and Bates, N. R. 2002. Interannual variability in the North Atlantic carbon sink. *Science* **298**, 2374–2378.

Kalnay, E., Kanamitsu, M., Kistler, R., Collins, W., Deaven, D. et al. 1996. The NCEP/NCAR 40 year reanalysis project. *B. Am. Meteorol. Soc.* **77**, 437–471.

Lee, K., Wanninkhof, R., Takahashi, T., Doney, S. C. and Feely, R. A. 1998. Low interannual variability in recent oceanic uptake of atmospheric carbon dioxide. *Nature* **396**, 155–159.

Le Quéré, C., Aumont, O., Bopp, L., Bousquet, P., Ciais, P. et al. 2003. Two decades of ocean CO_2 sink and variability. *Tellus* **55B**, 649–656.

Le Quéré, C., Orr, J. C., Monfray, P. and Aumont, O. 2000. Interannual variability of the oceanic sink of CO_2 from 1979 through 1997. *Global Biogeochem. Cycles* **14**, 1247–1265.

Liss, P. S. and Merlivat, L. 1986. Air-sea gas exchange rates: introduction and synthesis. In: *The role of air–sea exchange in geochemical cycling* (ed.P. Buat-Ménard). Riedel, Norwell, MA, 113–129.

Louanchi, F. and Hoppema, M. 2000. Interannual variations of the Antarctic Ocean CO_2 uptake from 1986 to 1994. *Mar. Chem.* **72**, 103–114.

Marland, G. and Boden, T. 2001. The increasing concentration of atmospheric CO_2, how much, when and why? *Erice International Seminar on Planetary Emergencies, 26th Session, Erice, Sicily, Italy, 19–24 August 2001*. Available online at http://cdiac.ornl.gov/

Nelson, N. B., Bates, N. R., Siegel, D. A. and Michaels, A. F. 2001. Spatial variability of the CO_2 sink in the Sargasso Sea. *Deep Sea Res. II* **48**, 1801–1821.

Obata, A. and Kitamura, Y. 2003. Interannual variability of the air–sea exchange of CO_2 from 1961 to 1998 simulated with a global ocean circulation-biogeochemistry model. *J. Geophys. Res.* **108**. doi:10.1029/2001JC001088.

Olsen, A., Bellerby, R. G. J., Johannessen, T., Omar, A. M. and Skjelvan, I. 2003. Interannual variability in the wintertime air–sea flux of carbon dioxide in the northern North Atlantic, 1981–2001. *Deep Sea Res. I* **50**, 1323–1338.

Olsen, A., Triñanes, J. and Wanninkhof, R. 2004. Sea-air flux of CO_2 in the Caribbean Sea estimated using in situ and remote sensing data. *Remote Sens. Environ.* **89**, 309–325.

Reynolds, R. and Smith, T. 1994. Improved global sea surface temperature analyses. *J. Clim.* **7**, 929–948.

Ropelewski, C. F. and Jones, P. D. 1987. An extension of the Tahiti–Darwin Southern Oscillation Index. *Mon. Weather Rev.* **115**, 2161–2165.

Smith, S. R., Legler, D. M. and Verzone, V. 2001. Quantifying uncertainties in NCEP reanalyses using high quality research vessel observations. *J. Clim.* **14**, 4062–4072.

Takahashi, T., Sutherland, S. C., Sweeney, C., Poisson, A., Metzl, N. et al. 2002. Global sea–air CO_2 flux based on climatological surface ocean pCO_2, and seasonal biological and temperature effects. *Deep Sea Res. II* **49**, 1601–1622.

Thompson, D. W. J. and Wallace, J. M., 2000. Annular modes in the extratropical circulation. Part I: month-to-month variability. *J. Clim.* **13**, 1000–1016.

Van Loon, H. and Madden, R. A. 1981. The Southern Oscillation. Part I: Global associations with pressure and temperature in northern winter. *Mon. Weather Rev.* **109**, 1150–1162.

Wanninkhof, R. 1992. Relationship between wind speed and gas exchange over the ocean. *J. Geophys. Res.* **97**, 7373–7382.

Wanninkhof, R., Doney, S. C., Takahashi, T. and McGillis, W. R. 2002. The effect of using time-averaged winds on regional air-sea CO_2 fluxes. In: *Gas Transfer at Water Surfaces*, American Geophysical Union Geophysical Monograph 127 (eds M. A. Donelan, W. M. Drennan, E. S. Saltzman and R. Wanninkhof). AGU, Washington, DC, 351–356.

Wanninkhof, R. and McGillis, W. R. 1999. A cubic relationship between air-sea CO_2 exchange and wind speed. *Geophys. Res. Lett.* **26**, 1889–1892.

Wentz, F. J., Peteherych, S. and Thomas, L. A. 1984. A model function for ocean radar cross sections at 14.6 GHz. *J. Geophys. Res.* **89**, 3689–3704.